INSPECTION OF SIC_f/SIC CERAMIC MATRIX COMPOSITE SPECIMENS EMPLOYED FOR FATIGUE EXPERIMENTS VIA LABORATORY X-RAY COMPUTED MICROTOMOGRAPHY

Z. QUINEY [1], M.R. BACHE [1], J.P. JONES [1]
[1] Swansea University Institute of Structural Materials, Swansea University, Bay Campus, Fabian Way, Crymlin Burrows, Swansea, SA1 8EN, United Kingdom
z.a.quiney@swansea.ac.uk
m.r.bache@swansea.ac.uk
jonathan.p.jones@swansea.ac.uk

Abstract. Hi-Nicalon SiC_f/SiC ceramic matrix composite (CMC) specimens have been inspected using laboratory based X-ray computed micro-tomography (µCT) both prior and subsequent to isothermal fatigue assessment. The fatigue specimens were in the form of a dog bone-shaped geometry with a minimum cross-sectional area of 40mm^2. Pre-test µCT inspections were conducted to identify the subsurface composite architecture and locate associated features introduced during the manufacturing process (e.g. isolated or conjoined porosity, matrix or interface discontinuities etc.). These µCT scans were subsequently correlated with matching post-test volumes in an attempt to determine the influence of such features upon damage accumulation and the ultimate failure position and cyclic damage mode(s).

The relationship between µCT scan resolution and identification of critical features is also discussed. In typical cone-beam X-ray systems, resolution is proportional to the source-to-specimen distance, but for efficiency may also be chosen so as to minimise the number of scans needed to capture the whole area of interest. The investigations are intended to provide input into the future development of an in situ mechanical testing µCT facility using lab-based X-ray systems.

1. Introduction

Due to lower relative density, superior mechanical performance at high temperature and resistance to environmental factors [1, 2], ceramic matrix composite (CMC) materials offer great potential for use in next-generation, low-emission aerospace applications. In order to realise this, a detailed understanding of their complex static and fatigue behaviour is required. This behaviour may be affected by macroscopic and microscopic processing artefacts contained within the material as a result of the multi-stage manufacturing procedure, and non-destructive evaluation (NDE) techniques can be used to identify their form and extent. Through repeated inspection of laboratory specimens prior to and subsequent to fatigue testing, the effect of manufacturing features upon the nature and location of ultimate failure can be characterised.

The manufacture of SiC fibre reinforced SiC matrix (SiC_f/SiC) CMCs like those used in the present study is described by Ruggles-Wren [3]. Typical features encountered in various forms of these materials include large individual and interconnected voids, delamination, interface debonding, matrix cracks and micro-porosity [4].

A range of NDE techniques can be applied to CMCs, and several articles can be found in the literature comparing their relative merits [1, 4, 5]. Technological advances and the introduction of commercially available systems have promoted X-ray computed micro-tomography (µCT) as the preferred method for the characterisation of various composite materials, due to superior image resolution and the ability to characterise internal features in three dimensions (3D). Cited examples can generally be divided into those utilising synchrotron radiation (SR) sources and those utilising laboratory-based divergent-beam X-ray sources. Bull et al [6, 7] compared the performance of a commercially available Nikon Metrology HMX 225 (divergent-beam) CT system with SR CT, achieving voxel resolutions of 4.3 and 1.4 µm, and overall scan times of 150 and 5 minutes respectively. SR can achieve resolutions as high as 0.5 µm [8]. The primary disadvantage of SR, however, is that it can only be produced at dedicated particle accelerator facilities. Alternatively, laboratory-based systems are still capable of identifying the vast majority of processing features and operational damage in composites [9].

Recent trends are in the direction of in situ µCT, which allows progression of damage to be tracked via a series of periodic tomographic scans in a bespoke mechanical testing device without the need for specimen removal and load train re-assembly. Such research typically utilises specialised facilities at SR sources [10-14], although some test devices have been integrated within laboratory X-ray CT systems [15-17]. Digital volume correlation (DVC) software can be used to quantify the damage accumulation between successive scans [17, 18].

This paper investigates the suitability of a laboratory-based system for correlating µCT scans and identifying damage in SiC_f/SiC CMC specimens. Inspections were conducted both prior and subsequent to fatigue assessment, to determine whether damage can be linked to specific manufacturing features. Additionally, the CT resolution and, consequently, form and size of feature that can be detected in the current specimen geometry will help determine the viability of future laboratory-based in situ characterisation.

2. Material and Experimental Details

The composition and manufacture of the SiC_f/SiC CMC material was similar to that described in reference [3], reducing the nominal overall porosity to less than ~2–3%. Dog bone style specimens, Fig.1, were cut from flat panels of approximate dimensions 230 x 150 x 5mm.

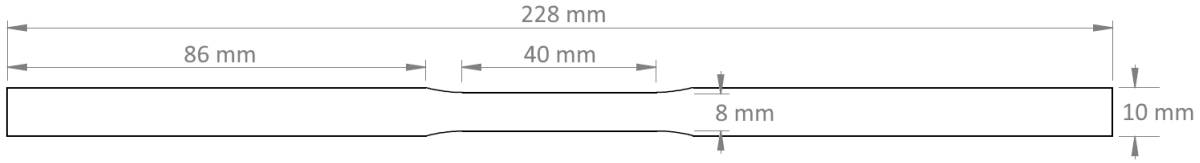

Fig. 1: CMC fatigue specimen geometry

X-ray µCT was carried out using an X-Tek HMX ST 225 kV system. The divergent-beam X-ray source had a minimum focal spot size of 5-10 µm, maximum energy of 225 kV and maximum current of 2 mA. A filtering material may be used to reduce polychromatic X-ray beam noise that can contribute to image artefacts such as beam

hardening [19]. A 4 megapixel, 16-bit detector provided high resolution images, which were reconstructed into a 3D volume file using a filter back projection algorithm, and viewed in Volume Graphics' "VG Studio MAX" software.

Due to the divergent-beam, and in contrast to SR, resolution is proportional to the source-to-specimen distance. This distance is set according to the region of interest (ROI) that must fit within the detector limits. Concerns over the potential presence of large void spaces within the tab (grip) section of specimens, initially meant that the entire specimen volume was scanned. The ROI was selected to include half of the specimen, and separate scans were completed for top and bottom halves. In these cases image resolution was 64 µm per voxel. This was later altered so that the ROI contained only the central, parallel gauge section in a single scan, at a resolution of 31 µm; i.e. the tab sections were ignored.

Subsequent to mechanical testing, post-test µCT was carried out by stacking both portions of the fractured specimen back-to-back and performing a single scan where the ROI included only the gauge section. Depending upon the position of the fracture, the ROI differed slightly for each specimen and resolution varied from 17–28 µm. Fig.2 demonstrates the ROI selected for different scan and specimen conditions. For image viewing purposes, the two portions were isolated and rotated back into their original orientation within the VG Studio MAX software.

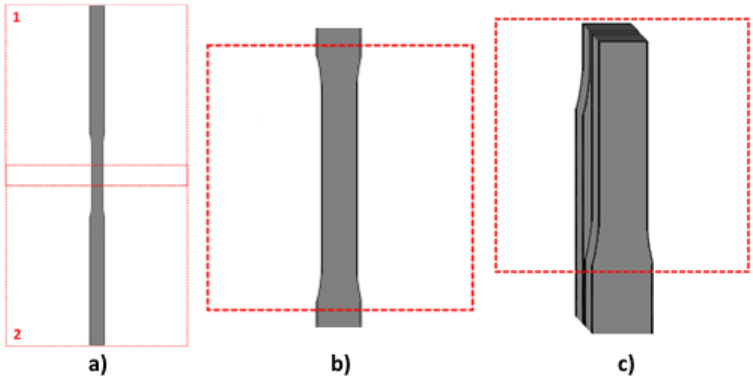

Fig. 2: Specimen ROI configurations for µCT: a) separate pre-mechanical test scans of top half (1) and bottom half (2) with overlap, b) single pre-mechanical test scan of gauge section, c) single post-mechanical test scan of fractured portions.

Isothermal fatigue testing was performed using an Instron 1362 servo-electrical machine fitted with water-cooled hydraulic wedge grips and a three-zone radiant lamp furnace. Zero to maximum (R=0), constant amplitude, load controlled fatigue cycles incorporated 1 second linear rise and fall ramps with a 60 second dwell at maximum stress. The maximum stress applied to different specimens ranged from 140 to 190 MPa. The criterion for fatigue run-out was set at 10^4 cycles. Details of test parameters are summarised in Table 1, but it is emphasised that the focus of this paper is NDE rather than the fatigue aspect of the research programme.

Table 1: Fatigue test details

Specimen	Temp (°C)	Stress (MPa)		Failed	No. cycles
		Min	Max		
CMC007	800	0	140	No	10000
CMC008	800	0	155	Yes	5493
CMC009	800	0	170	Yes	1776
CMC010	550	0	170	No	10000
CMC011	550	0	155	No	10000
CMC012	800	0	155	Yes	5272
CMC013	550	0	170	No	10000
CMC014	550	0	162.5	No	10000
CMC015	800	0	170	Yes	1744
CMC016	800	0	165	Yes	3458
CMC018	800	0	175	Yes	788
CMC019	550	0	175	Yes	7974
CMC020	550	0	180	Yes	7870
CMC021	550	0	190	Yes	1549

3. Results

3.1 Pre-Mechanical Test Characterisation

Upon completion of each CT scan of the pre-tested mechanical test coupons, the 3D volume file was reconstructed and manually inspected as a series of 2D cross-sectional 'slices' through the *x*, *y* and *z* planes. The primary features of interest were isolated or inter-connected internal voids, and these were observed to vary significantly in size between specimens. Each specimen was therefore graded I–III according to a simple measurement criterion based upon the largest void region from the 2D image; Grade I: where voids were too small to measure accurately (i.e. <<1 mm); Grade II: voids could be encircled within a diameter of 6 mm; Grade III: voids exceeded a 6 mm diameter region. Measurements were taken within the parallel gauge section only; results are shown in table 2.

Further quantification of the void characteristics was carried out using the 'Defect Detection' module of VG Studio MAX. Void detection is based on the variation in greyscale values of individual voxels in the volume file (a direct consequence of density disparity in the physical specimen), thus requires careful handling of threshold values which are specific to individual CT scans. Minimum and maximum void volumes to be included in the detection were set at 1 μm^3 and 20 mm^3 respectively. Porosity is the percentage total void volume within the ROI, which was restricted to the parallel gauge section. Results are shown in table 2.

Three outputs of the void analysis are necessary to understand the nature of the void space. The % porosity indicates the presence of large voids in extreme cases such as specimen CMC010 but does not necessarily correlate with largest void size in grade I and grade II specimens. Largest void volume understandably correlates well with grade in all cases, and shows an inverse correlation with number of voids; low numbers of voids indicates that porosity is inter-connected, forming much larger distinct void spaces. Visualisation of the typical void characteristics for each grade of specimen is shown in Fig. 3.

Numerous elongated void spaces could also be observed along fibre tows, likely to be caused by insufficient matrix infiltration between fibres or lack of bonding between fibre bundles and matrix. These could be observed when the voxel resolution was 64 µm, but had greater clarity when the resolution was improved (Fig. 4). These "crack-like discontinuities" could be mistaken for mechanically induced cracks or delamination when detected post fatigue testing, thus it is vital to identify their existence via pre-mechanical test characterisation to avoid misinterpretation during inspection of loaded specimens.

Table 2: µCT setup details and analysis results

Specimen	CT Scan Setup				Grade	Void Analysis		
	Energy (kV)	Current (µA)	Filter	Voxel Resolution (µm)		No. voids	Largest void (mm^3)	Porosity (%)
CMC007	90	200	None	67	I	127	0.017	0.036
CMC008	90	200	None	67	I	250	0.036	0.076
CMC009	90	200	None	67	II	168	0.519	0.185
CMC010	90	200	None	67	III	78	10.228	0.932
CMC011	90	200	None	67	II	144	0.221	0.139
CMC012	90	200	None	67	II	89	0.558	0.207
CMC013	90	200	Al (1mm)	64	I	671	0.042	0.214
CMC014	90	200	Al (1mm)	64	I	918	0.099	0.304
CMC015	90	200	Al (1mm)	64	I	821	0.065	0.270
CMC016	90	200	Al (1mm)	64	I	362	0.073	0.118
CMC018	90	200	Al (1mm)	64	I	391	0.042	0.106
CMC019	90	200	Al (1mm)	31	I	184	0.014	0.022
CMC020	90	200	Al (1mm)	31	I	323	0.016	0.039
CMC021	90	200	Al (1mm)	31	I	353	0.019	0.044

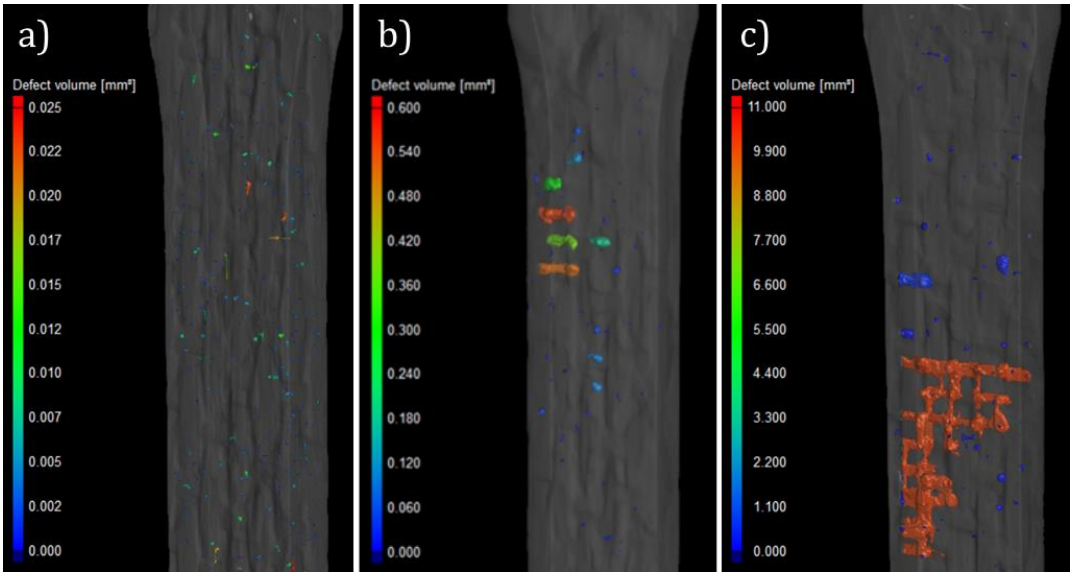

Fig. 3: Examples of pre-mechanical test specimens of a) grade I, b) grade II, c) grade III.

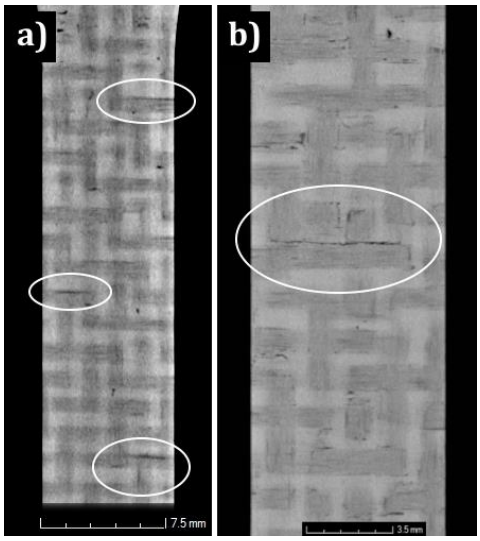

Fig. 4: Observations of "crack like discontinuities" associated with fibre tows viewed at a) 64 µm resolution, b) 31 µm resolution.

3.2 Post-Mechanical Test Characterisation

The plane of fatigue fracture varied between specimens, but was always within the 40 mm parallel gauge section. Some specimens failed close to the transition shoulder, while others such as CMC021 (Fig. 5) failed very close to the centre of the gauge length. An angled overview of this fracture is presented in Fig. 5a, indicating a relatively flat fracture orthogonal to the tensile loading axis (vertical to the page). The extent of fibre pull out parallel to the tensile axis is notably restricted. A single macroscopic step across the width of the gauge appears to be the result of the crack path deviating through the gauge thickness and governed by the 90^{o} fibre bundles. The interface between these transverse fibre bundles and the matrix seems to provide a weak link for cracking, as viewed from the front of the specimen on a near surface plane in Fig. 5b.

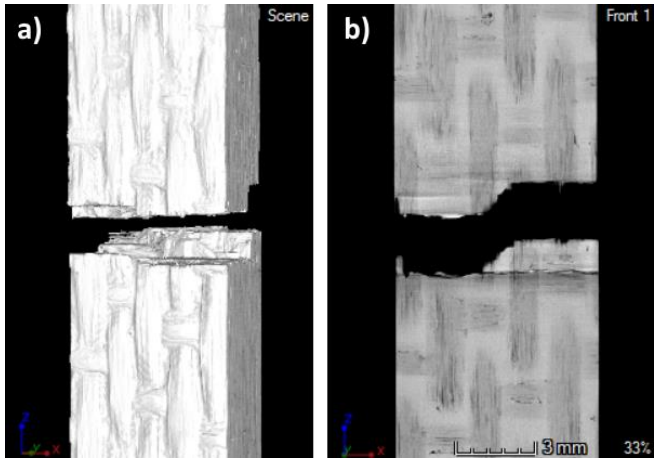

Fig. 5: Post-mechanical test µCT inspection of specimen CMC021 at 17 µm resolution; a) angled overview, b) front view.

Image correlation was performed by viewing pre and post-mechanical test µCT inspection files simultaneously on separate display screens. The eventual region of fracture was identified in the pre-test scan using distance measurement tools and unique void shapes as a reference. Both volume files were then analysed slice-by-slice to determine whether processing anomalies highlighted in the pre-test inspections were implicated in the onset of fatigue fracture.

The specific influence of matrix voids and porosity was investigated. The failures observed in numerous specimens appear to indicate that large voids found in grade II specimens had no direct influence upon the fracture location. In some cases, such as CMC012 imaged in Fig. 6, although the damage zone was adjacent to a region of dense void concentration, cracking did not initiate or intersect with any of the significant voids.

Whilst the emphasis of the present paper was to describe the qualitative relationship between processing features, our ability to identify such features, and ultimately their relationship to fatigue damage mechanisms, allows for early attempts at correlating features to fatigue life. To this end it is interesting to compare and contrast two specimens, both tested under fatigue at 550^{o}C. Specimen CMC010 contained the largest, single, interconnecting pore amongst the whole batch of specimens at 10.23mm^{3}, more than an order of magnitude greater than the largest pore in any other specimen, Fig. 7. This specimen actually achieved the run out condition of 10,000 fatigue cycles at a peak stress of 170MPa without fracture. In contrast, specimen CMC019, with a maximum pore size of 0.014mm^{3} and the smallest detected amongst the batch reported here, failed at a life of 7,974 cycles despite being tested at a peak stress just 5MPa greater. Obviously, it is impossible to say for how much longer specimen CMC10 would have resisted failure and whether the significant porosity illustrated in Fig. 7 would have been implicated in the

onset of fracture, certainly no new damage was detected via µCT inspection at the termination of the fatigue test. However, this example goes some way to emphasise the stochastic mechanical performance of these types of ceramic matrix composites, as well as the indeterminate relationship between defects and fatigue performance.

Grade I specimens, with CMC19 as a good example, indicated limited correlation between voids and failure. Occasionally the crack path interacted with a pre-existing void, Fig. 8, however, it was impossible to define the temporal relationship between the pore and failure mechanism, i.e. did the pore initiate cracking or interact with the crack growth?

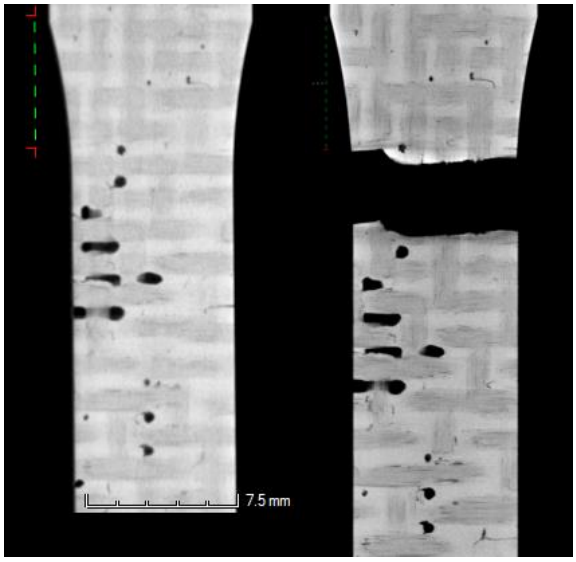

Fig. 6: Pre-mechanical test (left) and post-test (right) µCT inspections of specimen CMC012 (resolution = 67 µm and 28 µm respectively)

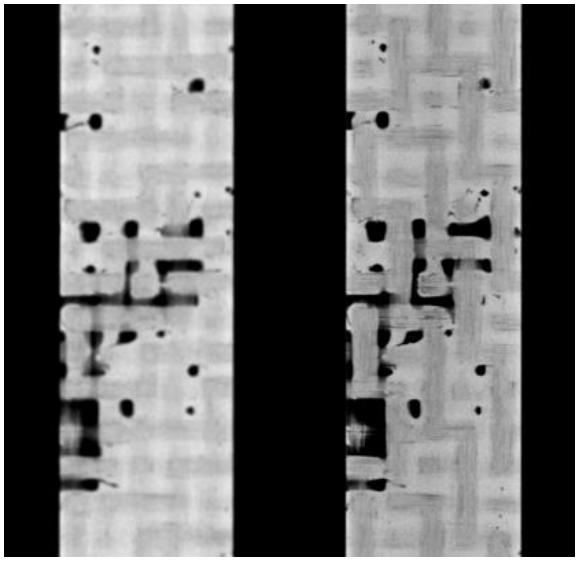

Fig. 7: Pre-mechanical test (left) and post-test (right) µCT inspections of specimen CMC010 (resolution = 67 µm and 31 µm respectively)

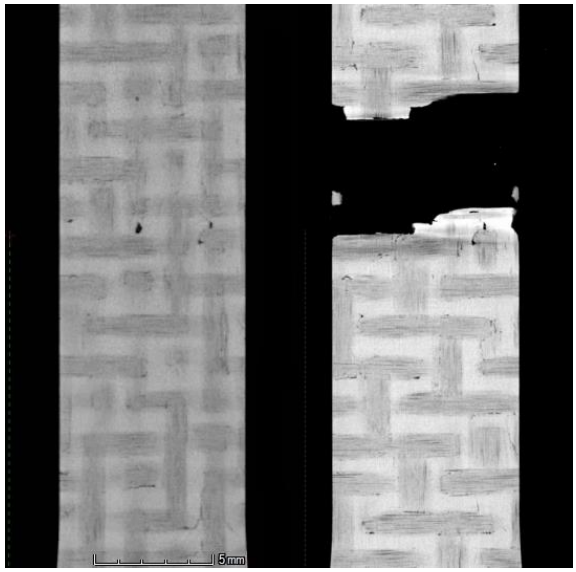

Fig. 8: Pre-mechanical test (left) and post-test (right) µCT inspections of specimen CMC019 (resolution = 31 µm and 20 µm respectively)

In the main, post processing crack like discontinuities, as previously highlighted in Fig. 4, did not appear to act as potent sites for true crack initiation. For example, Fig. 9 highlights that a discontinuity noted during a pre-mechanical inspection appears unaltered in the post-test inspection, despite the plane of ultimate fracture occurring just a few millimetres below. However, when the same specimen was inspected through the thickness

on a different vertical plane a similar sub-surface discontinuity was observed which appears to be the initiation site for ultimate failure (Fig. 10).

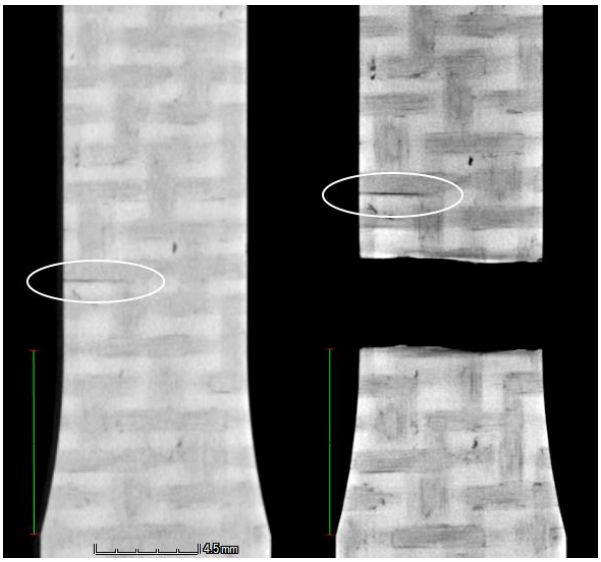

Fig. 9: Pre-mechanical test (left) and post-test (right) µCT inspections of specimen CMC008 (resolution = 67 µm and 27 µm respectively).

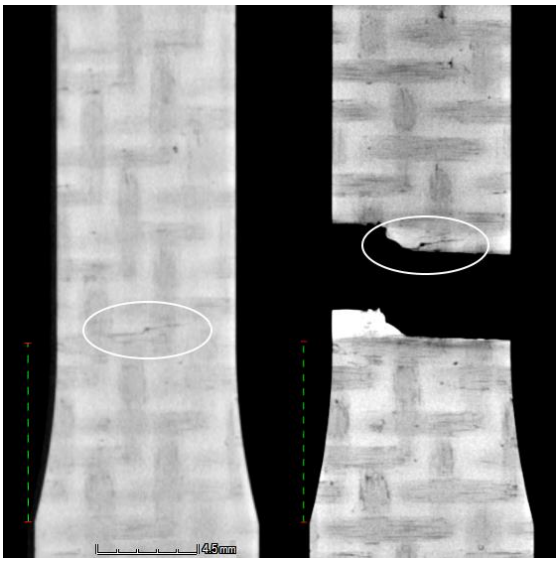

Fig. 10: Pre-mechanical test (left) and post-test (right) µCT inspections of specimen CMC008 (resolution = 67 µm and 27 µm respectively).

Finally, Fig. 11 illustrates specimen CMC020 where the ultimate plane of fracture was again close to the centre of the gauge length. A secondary fatigue crack was detected in the post-mechanical µCT inspection some 14 mm away from the main fracture. This indicates that fatigue damage can initiate at multiple locations before a single dominant crack, or network of cracks, causes the ultimate failure. The sub-critical fatigue crack clearly differs from the process discontinuities as it traverses both 0° orientated fibre bundles and the matrix. No feature was indicated at the corresponding location prior to mechanical testing. The crack was detected on numerous sub-surface images, helping to define a quarter elliptical profile at the corner of the gauge section, 1.5 mm through the thickness of the section and 5.5 mm in front surface length.

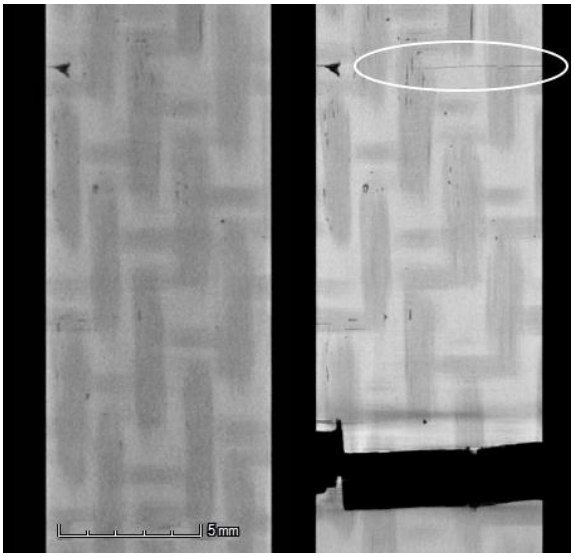

Fig. 11: Pre-mechanical test (left) and post-test (right) µCT inspections of specimen CMC020 (resolution = 31 µm and 17 µm respectively).

4. Conclusions

Laboratory-based X-ray µCT is the pre-eminent technique for characterising the as processed architecture of SiC_f/SiC CMC materials. Post processing features including isolated and inter-connected porosity within the matrix and fibre bundles can be resolved accurately. These can be comfortably detected at a system resolution of 67 µm, although clarity was greatly improved at 31 µm. Size and concentration of void space within the current batch of materials varied significantly.

Comparisons between images recorded prior to mechanical evaluation and post-test, in this case elevated temperature fatigue testing, failed to provide a definitive correlation between processing features and crack initiation. Grading of test coupons according to volume fraction of inherent porosity did not provide a direct relationship to fatigue performance, although it is recognised that the scale of the test matrix completed to date was limited. Evidence of multiple fatigue cracks could be found in failed inspections at 17 µm system resolution, but the precise mechanism of their initiation could not be identified. Higher resolution inspections may prove to be more revealing, but this would require the ROI to be subdivided into multiple scans at increased time and cost. These issues must be considered if designing a future in situ X-ray µCT facility capable of inspecting for damage accumulation whilst the specimen remains loaded in the test frame.

5. Acknowledgements

The current research was conducted under the Aerospace Technology Institute (ATI) initiative, funded by Innovate UK and Rolls-Royce plc (research contract 113017, SILOET II Work Package 19). Computed tomography inspections utilised facilities at the TWI Technology Centre, Port Talbot, Wales.

6. References

1. Harris, B., *Engineering Composite Materials*. 1999, London: Institute of Materials.
2. *Tensile Testing (2nd Edition) - Tensile Testing of Ceramics and Ceramic Matrix Composites*, in *Tensile Testing (2nd Edition)*, J.R.D. Associates, Editor. 2004, ASM Intl.
3. Ruggles-Wrenn, M.B., et al., *Effect of frequency and environment on fatigue behavior of a CVI SiC/SiC ceramic matrix composite at 1200°C.* Composites Science and Technology, 2011. **71**(2): p. 190-196.
4. Johnston, R.E., et al., *Investigation of Non-Destructive Evaluation Methods Applied to Oxide/Oxide Fiber Reinforced Ceramic Matrix Composite.* Mechanical Properties and Performance of Engineering Ceramics and Composites VII, 2012. **33**(2): p. 57-67.
5. Gyekenyesi, A., *Techniques for monitoring damage in ceramic matrix composites.* Journal of Intelligent Material Systems and Structures, 2013. **25**(13): p. 1531-1540.
6. Bull, D.J., et al., *A comparison of multi-scale 3D X-ray tomographic inspection techniques for assessing carbon fibre composite impact damage.* Composites Science and Technology, 2013. **75**: p. 55-61.
7. Bull, D.J., I. Sinclair, and S.M. Spearing, *Partial volume correction for approximating crack opening displacements in CFRP material obtained from micro-focus X-ray CT scans.* Composites Science and Technology, 2013. **81**: p. 9-16.
8. Bale, H., et al., *Characterizing Three-Dimensional Textile Ceramic Composites Using Synchrotron X-Ray Micro-Computed-Tomography.* Journal of the American Ceramic Society, 2012. **95**(1): p. 392-402.
9. Awaja, F., et al., *The investigation of inner structural damage of UV and heat degraded polymer composites using X-ray micro CT.* Composites Part A: Applied Science and Manufacturing, 2011. **42**(4): p. 408-418.
10. Aroush, D.R.-B., et al., *A study of fracture of unidirectional composites using in situ high-resolution synchrotron X-ray microtomography.* Composites Science and Technology, 2006. **66**(10): p. 1348-1353.

11. Chateau, C., et al., *In situ X-ray microtomography characterization of damage in SiCf/SiC minicomposites.* Composites Science and Technology, 2011. **71**(6): p. 916-924.
12. Scott, A.E., et al., *In situ fibre fracture measurement in carbon–epoxy laminates using high resolution computed tomography.* Composites Science and Technology, 2011. **71**(12): p. 1471-1477.
13. Wright, P., et al., *High resolution tomographic imaging and modelling of notch tip damage in a laminated composite.* Composites Science and Technology, 2010. **70**(10): p. 1444-1452.
14. Bale, H.A., et al., *Real-time quantitative imaging of failure events in materials under load at temperatures above 1,600 °C.* Nature Materials, 2013. **12**: p. 40-46.
15. Hufenbach, W., et al., *A test device for damage characterisation of composites based on in situ computed tomography.* Composites Science and Technology, 2012. **72**(12): p. 1361-1367.
16. Buffiere, J.Y., et al., *In Situ Experiments with X ray Tomography: an Attractive Tool for Experimental Mechanics.* Experimental Mechanics, 2010. **50**(3): p. 289-305.
17. Brault, R., et al., *In-situ Analysis of Laminated Composite Materials by X-ray Micro-Computed Tomography and Digital Volume Correlation.* Experimental Mechanics, 2013. **53**(7): p. 1143-1151.
18. Marrow, J., et al., *3D Studies of Damage by Combined X-ray Tomography and Digital Volume Correlation.* Procedia Materials Science, 2014. **3**: p. 1554-1559.
19. Dewulf, W., Y. Tan, and K. Kiekens, *Sense and non-sense of beam hardening correction in CT metrology.* CIRP Annals - Manufacturing Technology, 2012. **61**(1): p. 495-498.